RSC Advances

ROYAL SOCIETY OF CHEMISTRY

www.rsc.org/advances

Methanol formation by catalytic hydrogenation of CO_2 on nitrogen doped zinc oxide surface: An evaluative study on the mechanistic pathway by density functional theory

Ramasamy Shanmugam,[†,‡] Arunachalam Thamaraichelvan,[†] and

BalasubramanianViswanathan,*, [‡]

[†]Department of Chemistry, Thiagarajar College, Madurai, Tamilnadu 6250 09, India

[‡]National Center for Catalysis Research, Indian Institute of Technology Madras, Chennai, Tamilnadu 600 036, India

*E-mail: bvnathan@iitm.ac.in

Abstract

Investigation of the nature of adsorption of H_2O and CO_2 on nitrogen doped zinc oxide cluster surface and the resultant reaction between them has been performed using hybrid density functional theory (DFT) calculations at B3LYP level of theory in vacuum. The stable chemisorption modes of CO_2 and H_2O on metal, oxygen and nitrogen sites were examined. The calculated adsorption energies reveal that the formation of CO_2^- attached to N is the most favorable process for CO_2 on $Zn_{18}O_{17}$:N cluster surface with a binding energy of -1.86 eV. The water molecule spontaneously dissociates on the same surface to produce chemisorbed H* and *OH with the interaction energy of -0.77 eV. The model calculations rationalize the hydrogenation of CO_2 by H_2 generated from H_2O on the cluster surface. Thermodynamically favorable reaction pathways for the formation of methanol on the catalytic surface in vacuum were proposed. Among the three pathways, methanol formation follows the carbamate route. The carbamate formed, undergoes

hydrogenation to generate COOH* units followed by its exothermic dissection to *CO attached to N and *OH. Further hydrogenation of CO ultimately yields methanol. All the above steps were computationally evaluated.

Keywords: CO_2, H_2O, $Zn_{18}O_{17}$:N cluster, adsorption, hydrogenation, methanol formation, reaction pathways and density functional theory.

1. Introduction

Rapid increase in consumption of fossil fuels results in emission of huge amount of the greenhouse gas, carbon dioxide into the atmosphere. The radiative forcing effect of carbon dioxide causes adverse changes in the environment.[1] Partial success has been achieved in generating value added chemicals and fuels that can store renewable energies.[2-9] However, higher thermodynamic stability of CO_2 makes it relatively inert towards conversion process and thus requires activation. Among the metal oxide semiconductors, ZnO exhibits greater potential in activating inert CO_2 into active CO_2^- species on its surface.[10] The interaction of CO_2 and H_2O on ZnO surface has been studied extensively using DFT methods.[11-14] Although formation of carbonate and hydrogenated carbonate species on the surface has been confirmed, the fact that they restrict further activation has also been proved by *in situ* techniques.[15]

Industrially $Cu/ZnO/Al_2O_3$ was used as catalyst to synthesize methanol from a mixture of H_2, CO_2 and CO which requires high temperature and pressure.[16] On ZnO, photo reduction of CO_2 and H_2O yields methane as the major product[17] in contrast to the high temperature methanol synthesis on the catalytic surfaces. In sharp contrast, the enzyme carbonic anhydrase activates and fixes carbon dioxide as bicarbonate in nature

surprisingly at room temperature. It is better to produce chemicals rather than simply mimicking photosynthesis. Hence, based on photosynthetic enzyme model various possibilities were tried to use zinc complexes for CO_2 activation.[18-21] For solar energy conversion, semiconductor based photo catalytic systems have been employed in numerous applications which opened up a new era for the utilization of 43% of the available solar radiation in the visible range for hydrogen production from water as well as for CO_2 reduction.[8, 9, 17, 22-26] In recent years, Ni supported on SiO_2-Al_2O_3 has been used to produce methane using CO_2 and H_2 under solar energy conditions[27] while ZnO coated CuO yielded CO.[28] ZnO based catalysts have been shown to participate in the water splitting reaction too.[29, 30, 31] Further, ZnO being active in the UV region, undergoes photo corrosion during these reactions. For efficient reduction of CO_2, protons and electrons need to be continuously supplied during the reaction.

Nitrogen containing catalytic systems have recently received greater attention to overcome the above difficulty due to their greater potential to adsorb as well as activate carbon dioxide.[32-38] Nitrogen doped zinc oxide plays a vital role in catalysis, sensors, and optoelectronic devices.[39, 40] Further, N doped ZnO performs better than undoped catalyst in photocatalytic water splitting in the visible region.[41, 42] The activation of CO_2 mainly concerns with addition of an electron that alters the bond angle from linear 180° to near tetrahedral or triangular angle for formation of methanol and carbonate like products respectively. The N containing molecules in the homogenous catalytic systems lead to the O-C-O angle of 132° in the adjacent oxygen environment.[19] Hence, these kind of surfaces could provide a better environment for CO_2 activation.

The interactions of H_2O and CO_2 on various photo catalytic material surfaces have been extensively studied.[11, 13, 14, 43-51] The reduction of CO_2 by H_2O is controlled by surface configuration and adsorption strength of adsorbate on the active sites of a catalyst. The nature of interactions of CO_2 and H_2O on nitrogen doped zinc oxide surface has not yet been studied. Further, understanding of the basic molecular level interaction mechanism can provide new insight into design of a better catalyst. Hence, in the present study, a systematic investigation of the adsorption and activation of CO_2 and H_2O on nitrogen substituted stoichiometric ZnO nano cluster ($Zn_{18}O_{17}$:N) by means of DFT method is reported. Furthermore, the plausible reduction mechanism of CO_2 to methanol has also been attempted. We expect that this fundamental study would help to understand and identify the molecular events taking place on specific surfaces that are required to design newer and efficient catalysts for future reactions.

2. Molecular models and methods of computation

2.1. Creation of N doped stoichiometric $Zn_{18}O_{17}$:N cluster

Bulk ZnO crystallises in wurtzite structure. The surface was terminated with either oxygen or zinc sites with four fold coordination dominating over three or two fold analogues. Since surface relaxation alters the surface termination at nano level, both kinds of termination are possible on the surface.[52] For $Zn_{12}O_{12}$ cluster, the embedded ZnO $(000\bar{1})$ was used to study the interaction of CO_2 on the surface[13] which has many vacancies. Hence, to minimize the vacancies at the cluster level, $Zn_{18}O_{18}$ was chosen as the initial structure in order to account for stoichiometry, wurtzite configuration and

occurrence of Zn and O atoms in different coordination environments. This geometry was optimized and the resultant configuration is presented in **Figure 1.**

One of the fourfold sites of O was replaced by N to generate the stoichiometric $Zn_{18}O_{17}$:N, considered as a N doped ZnO model surface for computational studies. Introduction of N on ZnO surface creates the heterogeneity of atoms. Suitable modes of adsorption on metal oxides and nitrides were proposed for H_2O and CO_2.[44, 53-46, 47, 53] However, no such modes of adsorption are available for the corresponding nitrogen doped surface. Hence, new modes of adsorption on $Zn_{18}O_{17}$:N surface were proposed for H_2O and CO_2 combining those previously reported. Modes such as, on top (a) and (f) mono dentate linear (CO_2,η^1-O); (b) and (g) bent mono dentate (CO_2,η^1-C); (c) and (i) bridge bidentate (CO_2,η^2-C,O); (d) and (h) bridge tridentate (CO_2,η^3-O,C,O) and finally (e) and (j) bridge bidentate (CO_2,η^2-O,O), have been considered as adsorption models for CO_2. For water, (k) and (o) on top monodentate (H_2O, η^1-O); (l) on top monodentate (H_2O, η^1-H), (m), (n) and (p) bridge bidentate (H_2O, η^2-O,H) and finally (q) bridge bidentate (H_2O, η^2-H,H) modes of adsorption were proposed as models which are depicted in **Figure 2.**

The surface reconstruction during the adsorption process could provide more information on the surface reaction. For this reason, the adsorbates and cluster were allowed for full relaxation through geometry optimization. For clarity, the surface atoms with differing four, three and two fold coordinative sites are designated as 4fc, 3fc and 2fc respectively. In the adsorbed state, similar atoms in CO_2 and H_2O are labeled as O^a, O^b and O^w, H^a, H^b respectively in the results and discussion section.

2.2. Computational details

Geometry optimization and all other electronic calculations were computed employing Density Functional Theory (DFT) coupled with the gradient corrected B3LYP functional method. The electrons present in the Zn atom were treated with effective core potential of LANL2DZ.[54] For other atoms, aug-cc-pvdz[55] basis set was employed. Vibrational frequency calculations were carried out to identify and locate the intermediates corresponding to minima in the Potential Energy Surface that do not have any imaginary/negative vibrational frequency. The extent of interaction between the adsorbate and cluster was evaluated through calculation of interaction energy[56], $E_{ads} = E_{(adsorbate+cluster)} - (E_{adsorbate} + E_{cluster})$ where $E_{(adsorbate+cluster)}$, $E_{adsorbate}$ and $E_{cluster}$ are the Zero Point Energy (ZPE) corrected total energy of the adsorbate+cluster, bare adsorbate and cluster respectively.

Gibbs free energy for a given reaction step was calculated using the relation, $\Delta G^o = \sum G^o_{products} \_ \sum G^o_{reactants}$, where, $G^o_{reactants}$ and $G^o_{products}$ correspond to the ZPE corrected standard free energy (without any scaling factor) of reactants and products respectively at the temperature of 298.15 K and the pressure of 1 atm.

Ab initio molecular dynamics (AIMD) computation was performed using an extended lagrangian Atom Centered Density Matrix Propagation Molecular Dynamics (ADMPMD) at B3LYP/LANL2DZ level to check the stability of adsorbate on the surface. Final structure obtained from the optimized geometries of adsorbate with $Zn_{18}O_{17}$:N was chosen as the initial geometry for the ADMPMD run. Dynamics simulation was carried out at 1000 steps with the time scale of 0.1fempto second and the

fictitious electron mass of 0.1 amu. Thermostat temperature was maintained at 300K using velocity scaling method.[57]

Natural Bond Orbital (NBO) analysis[58] was used to characterize the charge transfer on the surface. All the electronic properties were computed using Gaussian09 software package[59]. The density of states was arrived at using spin polarized GGA-PBE method with the energy cut off of 380 eV and auto generated k points in CASTEP code implemented in Material Studio 5.5.[60]

3. Results and Discussion

3.1. $Zn_{18}O_{17}$:N geometries and chemical state of doped N

For nitrogen doped stoichiometric $Zn_{18}O_{17}$:N cluster, geometry optimization was performed using hybrid density functional theory. After finding the global minima configuration, the structural parameters were analyzed. The optimized configuration for $Zn_{18}O_{17}$:N is shown in **Figure 3(a)**. Upon doping of ZnO with N, the resulting cluster experienced modified structural parameters. Out of the four Zn-N bonds where N has 4fc, three are present on the same surface and have a bond distance of 2.04Å. However, the fourth one was elongated to a distance of 3.50Å thus indicating the absence of fourth bond. The presence of nitrogen in three fold coordinative site is favored and causes a slight expansion of the crystal. This effect was experimentally observed in ZnO doped with N leading to a small shift in the 2Θ value.[61] The bond length of Zn-O lies in the range of 1.93 to 1.99Å, the variation arising due to the surface relaxation of the atoms. Furthermore, the oxidation state of surface N was evaluated from the Partial Density of Sates (PDOS) of $Zn_{18}O_{17}$:N as shown in **Figure 4**. The overall DOS population of $Zn_{18}O_{17}$:N revealed a population profile similar to that observed in $Zn_{18}O_{18}$ thus

confirming the incorporation of N on the surface. ZnO does have N as N^{3-} which is isoelectronic with O^{2-} ion. This attributes excess of electron density on surface N in relation to oxide species which is confirmed from the spin density analysis of $Zn_{18}O_{17}$:N as depicted in **Figure 3(b).**

3.2. CO_2 adsorption on $Zn_{18}O_{17}$:N

The adsorption mode of CO_2 on nitrogen doped zinc oxide surface has not been known yet. Hence, ten different molecularly adsorbed predetermined configurations of CO_2 were chosen and relaxed. After finding the global minimum, the physisorption or chemisorption was characterized by calculating the adsorption energies. The structural parameters and adsorption energies for the selected configurations are presented in **Table 1.** For adsorption of CO_2 at zinc sites with varying coordinative environments on $Zn_{18}O_{17}$:N surface, the adsorption energies were computed using both CO_2,η^1-O and CO_2,η^1-C monodentate linear vertical to the surface modes. After relaxation, both the geometries yielded the same configuration as shown in **Figure 5(a)**.

The binding energies for the adsorption of CO_2 on metal sites in pure metal oxides have been shown to follow the weak Eley−Rideal physisorption model rather than chemisorption. The CO_2 was held on the surface without effective charge transfer from the surface. The structural parameters of CO_2 were not affected[62] and were indicative of free CO_2 in the gas phase **(Table 1(a)).** Thus, CO_2 does not get activated on metal sites in pure metal oxide frame work. However, when the interaction of bidentate and tridentate modes of CO_2 on coordinative unsaturated sites of oxygen, zinc and nitrogen of $Zn_{18}O_{17}$:N were considered, the chemisorption occurs. The resultant structures are

presented in **Figure 5(b &c)**. Adsorption of CO_2 (η^1.C) at the three fold coordination site, $O_{(3fc)}$, on the edge of the surface leads to the carbonate formation via the two oxygens coordinating with two adjacent $Zn_{(3fc)}$ sites thus saturating the surface oxygen vacancy[48] **(Figure 5(b))**. The angle of O-C-O bond was altered to 122.9° from 180° which is closer to triangular. The C-O^a and C-O^b bond lengths were elongated from 1.16 to 1.27 Å with the binding energy of -1.14eV. These values correlate well with the tridentate carbonate structure on ZnO surface[48]. In addition to evaluation of the charge donor/acceptor interactions, NBO charge analysis indicates that the charges on C, O^a and O^b acquired an excess value of -0.555 e indicating the effective interaction with the surface. The calculated vibrational frequencies have real values indicating the stable nature of the structures. The O-C-O asymmetric stretching mode occurs at 1580 cm^{-1}. The surface adsorbed CO_2 reveals the $O_{surface}$-C stretching at 1348 cm^{-1}, while the carbonate like three C-O units stretch at 1045 cm^{-1}. The decrease in C=O stretching is due to the loosening of the bond as a result of the adsorption through only one oxygen atom. The larger decrease in frequency in carbonate structure is experienced due to decrease in bond order in the two coordinating C=O groups. The out of plane bending mode of CO_2 occurs at 846 cm^{-1}. All calculated frequencies are consistent with the reported experimental values[15] and suggest that even if the surface has an impurity of N, the adsorption nature of oxide does not alter.

The binding energy of CO_2 in η^3 adsorption on $N_{(4fc)}$ is -1.86eV with a chemisorption distance of 1.35 Å for $N_{(4fc)}$-C. After the insertion of CO_2, the bonds surrounding N are broken. The upward movement of N atom reveals its dangling nature enhanced by greater adsorption. The two coordinatively unsaturated Zn atoms in the neighborhood are also

pushed upward to facilitate coordination with oxygen atoms with distances of O^a-Zn and O^b-Zn being 2.03Å and 2.04 Å respectively **(Figure 5(c))**. Further, the adsorption energy of the same mode on pure $Zn_{18}O_{18}$ was calculated **(supporting information 1)** to examine the effect of nitrogen. For pure $Zn_{18}O_{18}$ clusters, the value is -1.06 eV which is lower than that for N substituted surface by -0.80 eV. This result indicates that the presence of nitrogen enhances the adsorption.

Comparison of the adsorption energies reveals that the tridentate carbamate species is more favorable than carbonate species. It may be due to the greater electron density on N and its lower electronegativity than O which favor effective charge transfer. The Gibbs free energy profile is depicted in **Figure 6** for the above process. CO_2 interacts first with the surface by physisorption **(Figure 6, S1)**. Then the C interacts with N leading to distortion of the O-C-O angle **(Figure 6, S2).** The resultant bent configuration of the bidentate species has a relative Gibbs free energy of -0.77 eV. The values in the calculated vibrational frequencies show that this species is a transition state which undergoes further changes to form a stable tridentate species (**Figure 6, S3)**.

The excess charge on CO_2 is -0.738 e which is greater than that acquired on tridentate carbonate (-0.555 e). This charge transfer from the surface reveals that the N doped zinc oxide is a more powerful Lewis base than pure zinc oxide. In addition, there is no imaginary frequency in the vibrational spectrum that indicates its stable nature. The O^a-C-O^b asymmetric stretching mode occurs at 1461 cm^{-1}. The surface N-C stretching and the symmetric stretching that combines C-O and N-C are observed at 1366 cm^{-1} and 1063 cm^{-1} respectively. At 823 cm^{-1}, the out of plane bending of C in carboxylate is revealed. These patterns have also been observed in organic carbamate species.[63]

Further investigation of carbamate stability on the surface was done using ADMPMD calculation. The distance between carbamate and the surface at 300 K is shown in **supporting information Figure 1(a)**. The plot reveals that during the dynamical run, the adsorbed CO_2 is held on to the surface up to 1 ps without any desorption.

Density of states analysis provides information such as where exactly the surface transferred electrons are populated on the adsorbate. Thus, the partial density of states (PDOS) for s and p orbitals of CO_2 corresponding to free CO_2, physisorbed linear CO_2, tridentate carbonate and tridentate carbamate were plotted (**Figure 7)**. The PDOS population of CO_2 in the physisorbed state reveals that there is no effective interaction with the surface. For the tridentate carbonate species, the p orbital is more populated in the range of -7.5 eV to 0 eV at the fermi level. This indicates that the surface effectively transfers the charge to the adsorbate in the activated form. Although the tridentate carbamate has the same pattern, the population is higher than that of carbonate. Thus, activation in the presence of nitrogen is more facile than in pure oxide environment.

3.3. Adsorption of H_2O on $Zn_{18}O_{17}$:N

Presence of N produces a number of possible adsorption mode configurations suitable as active sites for H_2O on $Zn_{18}O_{17}$:N surface. To find the favorable sites for preliminary H_2O adsorption, numerous adsorption sites were inspected. As sites other than N behave similar to those of pure metal oxide, the atoms present around N in the surface have been considered as adsorption models for initial H_2O adsorption. On optimization, only three of them yielded thermodynamically favorable sites as shown in **Figure 8**. **Table 2** summarizes the structural parameters.

Using η2 (a) mode, adsorption leads to the auto dissociation of H_2O with the binding energy of 0.02 eV. This value suggests that the dissociation on N active site is slightly endothermic in nature. The H^a gets adsorbed on surface N and the O-H^b on adjacent Zn atom with the adsorption distance of 1.06 Å and 1.96 Å respectively. This correlates well with the dissociation of H_2O on $Ta_3N_5(100)$ surface.[46] Now the upwardly elongated N in the three fold coordinative site contracted to a distance of 2.37 Å from 3.50 Å with respect to bottom layer. Bond length of O-H^b was found to be 0.96 Å which is similar to bare free O-H distance in H_2O. The NBO charge analysis **(Table 2)** shows that the charge on N decreases from -1.469 e to -1.237 e while the charge on O increased from -0.958 e to -1.230 e indicating that the excess charge has been transferred from the surface, which causes the dissociation of a H atom.

IR frequencies revealed that there is no negative vibration in the frequencies indicating that the configuration is a minimum. The vibrational frequency values corresponding to O-H^a symmetric stretching at 3836 cm^{-1}, N-H^b symmetric stretching at 2885 cm^{-1}, (N-H^b+O-H^a) in plane wagging (1014 cm^{-1}), (N-H^b+O-H^a) out of plane wagging (1014 cm^{-1}) and O-H^a bent vibration (737 cm^{-1}) support the above observation.

Another favorable mode of adsorption of H_2O is using the coordination of both O and H atoms to the three fold coordinated Zn and O sites respectively in a vertical fashion as shown in **Figure 8(b).** The Zn atom, present adjacent to four fold coordinated Zn, was slightly displaced upward from the top layer and was held with a distance of 2.15 Å. The calculated binding energy of H_2O in the adsorbed state was -0.77 eV. The same kind of adsorption occurs for H_2O on Zn_2GeO_4 surface.[44] Bond lengths of O-H^a and O-H^b are 0.96 and 0.99 Å respectively. Bond distances of 2.15 Å for $Zn_{surface}$-O_{water} and 1.70 Å for

$O_{surface}$-H_{water} indicate weak adsorption. NBO charge analysis predicted the charge on individual O as -0.999 e, on H^a as 0.498 e and on H^b as 0.535 e revealing that there is no effective charge transfer from the surface to the adsorbate. The vibrational frequency analysis predicted stable configurations for all. The various frequencies calculated are: free O-H^b symmetric stretching (3841 cm^{-1}), adsorbed O-H^b, symmetric stretching (2984 cm^{-1}), O-H^a bending (1583 cm^{-1}) and O-H^b adsorbed bending (563 cm^{-1}).

The horizontal adsorption of H_2O on ZnO at corner site leads to the auto dissociation. The O-H^a was attached to $Zn_{(3fc)}$ and the H^b was attached to the adjacent $O_{(3fc)}$ with an adsorption energy of -0.44 eV as shown in **Figure 8(c).** This value is relatively higher than that of (a). The bond lengths are, O- H^a (0.96 Å) and $O_{surafce}$-H^b (1.00 Å). The vibrational frequencies suggest the existence of free $O_{surafce}$-H^b with a value of 3069 cm^{-1}. The stretching vibrations of chemisorbed O-H^a are observed at higher values than those for $O_{surface}$-H^b at 3851 cm^{-1} and O-H^b out of plane bending at 1020 cm^{-1}, all being positive.

In order to confirm the stability of the dissociatively adsorbed H_2O on the surface, ADMPMD run was computed, results of which are presented in **supporting information Figure 1(b)**. The plot reveals that the dissociated species were present on the surface up to 1 ps without desorption indicating the stability of the dissociated species on the surface.

To further evaluate the interaction of catalytic surface with H_2O, partial density of states for various configurations were investigated. In **Figure 9, (a), (b), (c) and (d)** represent free H_2O, dissociative adsorption at N site, molecular adsorption at metal-oxygen site and dissociative adsorption at metal-oxygen respectively. For dissociative

adsorption, the PDOS of (b) resembles that of (d) which indicates that the dissociation of water on both the sites is facilitated. Further, the population in (b) around fermi level is small. This helps effective electron charge transfer top orbital from the surface N. The molecularly adsorbed configuration (c) has overlapping of orbitals that are less populated than the dissociated species revealing that the molecular nature still exists on the surface.

Preceding the stage of hydrogenation, the source of hydrogen has to be predicted. The adsorption energies reveal that CO_2 gets competitively adsorbed on N active site on $Zn_{18}O_{17}$:N. The H_2O adsorption and dissociation is preferred on N site as well as oxide site. However, water was preferentially dissociating on the corner site of the cluster similar to the dissociation of water on pure oxide surface. Hence, the source of hydrogen was assumed to be from the corner vacant site.

3.4. Coadsorption of CO_2 and H_2O

H_2O hinders the adsorption of CO_2 by competing with it and leads to poisoning of the adsorbent. On the other hand, H_2O was used as reactant giving rise to the bicarbonate ion. Results obtained from the single molecule adsorption calculations on co-adsorption of CO_2 and H_2O were employed to verify the above fact by looking for any significant interaction on the surface. The bimolecular adsorption of water and carbon dioxide was carried out by choosing the stable configuration for the catalyst, placing one carbon dioxide adsorbed through carbon on surface N and water in the side on adsorption mode as initial configurations. Structural features of two modes **(Figure 10)** of co-adsorbed configuration surrounding the N substituted environment are presented in **Table 3**. The calculated binding energy shows that the carbamate configuration is more favorable in

the co-adsorption mode. In 10 (a) and (b), the water molecule coordinates in a bidentate fashion through H to O in (a) and N in (b) and O to the Zn.

The final configurations indicate that the η^1-C of CO_2 in (a) and (b) have bent structures and the water is in the side on adsorption mode with the total binding energies of -2.27 eV and -2.15 eV respectively. Both the molecules have retained their original configurations in (a) and (b) even though the adsorption modes are different, suggesting that the adsorption of CO_2 on N would facilitate the activation in the free as well as in the combined forms. The structural features of the water molecules are not altered in all the configurations. The CO_2 angle was altered to 122° which is lower by 5° than in the carbamate species. Thus, in the presence of water molecule, the adsorption and activation of CO_2 are more facilitated via hydrogen bonding like interactions that favor the adsorption.

After locating the global minima (a) configuration in **(Figure 10),** further stability and interaction of the species were evaluated using ADMPMD run method. The calculated ADMPMD profile is depicted in **supporting information Figure 1(c)**. The plot shows the coadsorbed H_2O and CO_2 on the surface are retained without migration from its adsorption site till 1 ps. This reveals that the surface water does not affect the chemisorbed CO_2 by forming bicarbonate related species.[15] Hence, in the mechanistic pathway studies, the water molecules were not included as it was assumed that there is no effect of water molecules.

3.5. Hydrogenation of CO_2

The hydrogenation of CO_2 to methanol was processed with various complex transition states and intermediates. On metal oxide surface, formation of carbonate, carboxylate and formate species have been proposed as intermediates for CO_2 reduction reactions depending on the reaction environment.[64, 65] Detailed reduction mechanisms are available for pure metals[66, 67] and metal oxides.[47, 67, 68] However, for N substituted metal oxides enough data are not available to understand the product formation. Hence, understanding the principal process involved in the hydrogenation of CO_2 by means of DFT mechanistic path way would predict the favorable configurations and give insight into the stability of products and transition states.

Since the active site for CO_2 reduction is N, the hydrogen would interact with the adjacent Zn and O sites on the surface. On these sites, H_2 heterolytic dissociation was favorable and H easily migrated due to the action of spillover.[69-71] The surface was covered with hydrogen and the effect of surface hydrogen on the reaction was negligible.[72] Hydrogenation of CO_2 by H_2 on ZnO surface has been reported.[51] Based on the above results, the following reaction pathway was proposed and tested for the methanol formation. The schematic representation of the mechanistic pathway is shown in **Figure 11.** Relative Gibbs free energy profile of hydrogenation of CO_2 to methanol is depicted in **Figure 12.** During the catalytic cycle, the reactant CO_2 was adsorbed on the catalytic surface and activated by chemisorption of on N as CO_2^- species.

The next step in the catalytic cycle is that the surface bound **(S1)** activated $*COO^-$ abstracts a proton on to carbamate oxygen forming a O-H bond.[64] As a result, the carboxylic acid group of η2-COOH* is present perpendicular to the surface, as shown in **Figure 11(S2)**. The relative Gibbs free energy was found to be -2.55 eV indicating the

spontaneous nature of the process with respect to free CO_2 and H_2. In another possibility based on the proton coupled electron transfer, the H added to C to form a foramte species. But the added H was found to instantly migrate to N. This indicates that the carbon valency was fully saturated by the surface bond. These results reveal that the proton would be easily added to the carbamate species and the formation of formate species was ruled out on the carbamate. The O^b-H was far away in **S2** from the surface and the carbonyl has the interaction with the nearby Zn atom which is slightly moved above the surface. The O^a-C-O^b angle of 117° suggests that the angle was stretched compared to the **S1** state. As per the proposed mechanism, there is a possibility of either dissociation of O^a-H in **S2** leading directly to **S4** or addition of H on O^b to form diol **(S3)** species. The diol is further eliminating H_2O to form **S4.** However, the relative free energy profile indicates that the COOH*(**S2**) capturing a proton (at the OH moiety) and releasing water is a more favorable route than the other one. This is due to the fact that compared to C-O^a bond (1.27 Å), the C-O^b (1.37 Å) is fairly weakened and favors the dissociation.

*CO remains chemisorbed on the surface **(S4)** with the relative Gibbs free energy of -2.40 eV which is more positive compared to **S2**. The $N_{surface}$-C-O^a angle was found to be 176.38° that makes it nearly parallel to the surface. The O^a was bonded to the adjacent $Zn_{(3fc)}$ atom in $N_{surface}$-C-O^a, revealing that the surface coordinative unsaturation is required for the stabilization of surface species. Better reduction of CO_2 requires the formation of CO species from *COOH that should be spontaneous in nature.[73] On oxide surface, formation of CO was difficult.[64] However, it is favored by N substitution in ZnO surface. Hence, the chemisorbed CO* alone is present on the surface **(S4)**.

Further attack of hydrogen on carbon is more favorable and yields a chemisorbed formyl species **(S5)** with the relative Gibbs free energy of -2.59 eV indicating the spontaneity of the reaction. The H-C-O angle is 115.6° and C-H as well as C-O distances are 1.11 Å and 1.27 Å respectively. Further attack of H leads to formation of H_2CO* species **(S6)** on the surface with the relative Gibbs free energy of -1.39 eV. This process is slightly exothermic in nature. Now, the hydride species present in the medium will react with oxygen to form methylene alcohol **(S7)** with a relative Gibbs free energy of -1.60 eV via a spontaneous and endothermic route. Attack of H on carbon in **S6** leads to the final product, methanol. Once the methanol is formed, the valences of the atoms are satisfied and during the optimization, they get relieved from the surface but held on to the surface by weak physical interaction **(S8).** On removal of methanol from surface, the active site is regenerated and is ready for further uptake of CO_2.

4. Conclusion

DFT calculations were carried out for the first time to explore the adsorption and activation of CO_2 and H_2O and the reduction mechanism of CO_2 to methanol by hydrogenation on $Zn_{18}O_{17}$:N model surfaces. The calculations were performed at B3LYP with all the plausible modes of adsorption. The most favorable mode of adsorption for CO_2 is through mono chemisorption via carbon on N and electrostatic interaction with neighboring oxygen atoms. The present study reveals that the CO_2 is activated to a greater extent with a bond angle of 127° in carbamate and 122° in the coadsorption of H_2O and CO_2. In case of H_2O, dissociative adsorption was favored. Presence of N enhanced the adsorption energies in relation to pure $Zn_{18}O_{18}$. Hydrogenation of CO_2 to CH_3OH proceeds through carbamate, carbonmonoxide, formyl, formaldehyde and

methylene alcohol. The results indicate that formation of CO via dissociation of carbamate rather than diol route required a barrier of -2.48 eV. Since all the reaction steps were associated with negative free energies, the methanol formation was achieved at lower cost than the conventional methods. Further studies on N containing defective surfaces may lead to more insight into methanol formation.

Acknowledgements

We acknowledge department of science and technology (DST), India, for setting up the National Centre for Catalysis Research (NCCR). The authors also acknowledge the high performance computing environment (HPCE), Indian Institute of Technology Madras (IITM) for providing computational facilities. The author R. S. is thankful to Council for Scientific Industrial Research (CSIR) for providing financial support vide., Ref. No. 08/117(0001)-2013-EMR-I.

References

1. P. Falkowski, *Science*, 2000, **290**, 291-296.
2. S. Toshiyasu, C. Jun-Chul and Y. Hiroyuki, *Chem. Rev.*, 2007, **107**, 2365−2387.
3. C. Graves, S. D. Ebbesen, M. Mogensen and K. S. Lackner, *Renew. Sust. Energy Rev.*, 2011, **15**, 1-23.
4. K. Huang, C.-L. Sun and Z.-J. Shi, *Chem. Soc. Rev.*, 2011, **40**, 2435-2452.
5. R. J. Pearson, M. D. Eisaman, J. W. G. Turner, P. P. Edwards, J. Zheng, V. L. Kuznetsov, K. A. Littau, L. di Marco and S. R. G. Taylor, *P. IEEE*, 2012, **100**, 440-460.
6. S. Enthaler, *ChemSusChem*, 2008, **1**, 801-804.
7. F. Joó, *ChemSusChem*, 2008, **1**, 805-808.
8. C. R. Somnath, K. V. Oomman, P. Maggie and A. G. Craig, *ACS Nano*, 2010, **4**, 1259–1278
9. S. N. Habisreutinger, L. Schmidt-Mende and J. K. Stolarczyk, *Angew. Chem. Int. Ed.*, 2013, **52**, 7372-7408.
10. H. J. Freund and M. W. Roberts, *Surf. Sci. Rep.*, 1996, **25**, 225-273.

11. J. B. L. Martins, V. Moliner, J. Andrés, E. Longo and C. A. Taft, *J. Mol. Struc-Theochem*, 1995, **330**, 347-351.
12. M. Casarin, C. Maccato and A. Vittadini, *Surf. Sci.*, 1997, **377–379**, 587-591.
13. K. Fink, *Phys. Chem. Chem. Phys.*, 2006, **8**, 1482-1489.
14. S. A. Farias, E. Longo, R. Gargano and J. B. Martins, *J. Mol. Model.*, 2013, **19**, 2069-2078.
15. N. Heshmat, W. l. Christof, M. Martin and W. Yuemin, *J. Phys. Chem. C*, 2011, **115**, 908–914.
16. Y. Zhang, Q. Sun, J. Deng, D. Wu and S. Chen, *Appl. Catal., A*, 1997, **158**, 105-120.
17. M. Watanabe, *Surf. Sci. Lett.*, 1992, **279**, L236-L242.
18. M. C. Curet-Arana, P. Meza, R. Irizarry and R. Soler, *Top. Catal.*, 2012, **55**, 260-266.
19. A. Fuchs, E. Kaifer, H. Wadepohl and H.-J. Himmel, *Eur. J. Inorg. Chem.*, 2012, **2012**, 4020-4028.
20. H.-J. Himmel, *Eur. J. Inorg. Chem.*, 2007, **2007**, 675-683.
21. R. Silaghi-Dumitrescu, M.-M. Uţă, A. Kallay and J. Bodis, *J. Mol. Struc-Theochem*, 2010, **942**, 15-18.
22. M. R. Hoffmann, S. T. Martin, W. Choi and D. W. Bahnemann, *Chem. Rev.*, 1995, **95**, 69-96.
23. C. Xiaobo, S. Shaohua, G. Liejin and S. M. Samuel, *Chem. Rev.*, 2010, **110**, 6503–6570.
24. K. Maeda, *J. Photochem. Photobiol.-C*, 2011, **12**, 237-268.
25. B. Kumar, M. Llorente, J. Froehlich, T. Dang, A. Sathrum and C. P. Kubiak, *Annu Rev Phys Chem*, 2012, **63**, 541-569.
26. A. Hironori, A. Michele, N. A. John, A. B. Mark, J. B. Eric, T. B. Alexis, E. B. John, C. Carol, D. Eckhard, A. D. David, D. Kazunari, L. D. Daniel, E. Juergen, F. Etsuko, H. G. Dorothy, A. G. William, D. W. Goodman, K. Jay, J. K. Gregory, H. K. Harold, E. L. James, E. M. Leo, J. M. Tobin, M. Keiji, M. N. Kenneth, P. Roy, Q. Lawrence, R.-N. Jens, M. H. S. Wolfgang, D. S. Lanny, S. Ayusman, A. S. Gabor, C. S. Peter, B. R. Stults and T. William, *Chem. Rev.*, 2001, **101**, 953−996.
27. F. Sastre, A. V. Puga, L. Liu, A. Corma and H. García, *J. Am. Chem. Soc.*, 2014, **136**, 6798-6801.
28. W.-N. Wang, F. Wu, Y. Myung, D. M. Niedzwiedzki, H. S. Im, J. Park, P. Banerjee and P. Biswas, *ACS Appl. Mater. Interfaces*, 2015, **7**, 5685-5692.
29. M. Zhong, Y. Ma, P. Oleynikov, K. Domen and J.-J. Delaunay, *Energy Environ. Sci.*, 2014, **7**, 1693-1699.
30. T. Wang, R. Lv, P. Zhang, C. Li and J. Gong, *Nanoscale*, 2015, **7**, 77-81.
31. A. Kushwaha and M. Aslam, *RSC Advances*, 2014, **4**, 20955-20963.
32. S. Schenk, J. Notni, U. Kohn, K. Wermann and E. Anders, *Dalton Trans*, 2006, DOI: 10.1039/b608534b, 4191-4206.
33. M. Ismael, R. Sahnoun, A. Suzuki, M. Koyama, H. Tsuboi, N. Hatakeyama, A. Endou, H. Takaba, M. Kubo, S. Shimizu, C. A. Del Carpio and A. Miyamoto, *Int. J. Greenh. Gas Control*, 2009, **3**, 612-616.
34. E. M. Mindrup and W. F. Schneider, *ChemSusChem*, 2010, **3**, 931-938.

35. F. d. S. Eirik and F. S. Hallvard, *Ind. Eng. Chem. Res.*, 2006, **45**, 2497–2504.
36. W. Conway, D. Fernandes, Y. Beyad, R. Burns, G. Lawrance, G. Puxty and M. Maeder, *J. Phys. Chem. A*, 2013, **117**, 806-813.
37. Y. Jiao, A. Du, Z. Zhu, V. Rudolph, G. Q. Lu and S. C. Smith, *Catal. Today*, 2011, **175**, 271-275.
38. G. T. Rochelle, *Science*, 2009, **325**, 1652-1654.
39. H. Qin, W. Li, Y. Xia and T. He, *ACS Appl. Mater. Interfaces*, 2011, **3**, 3152-3156.
40. K. Jindal, M. Tomar and V. Gupta, *Analyst*, 2013, **138**, 4353-4362.
41. Z. Xu, S. Chenghua, Y. Hua, C. Zhi Gang, X. Zheng, Y. Delai, L. Gao Qing, L. Xinyong and W. Lianzhou, *J. Phys. Chem. C*, 2013, **117**, 4937−4942.
42. A. P. Bhirud, S. D. Sathaye, R. P. Waichal, L. K. Nikam and B. B. Kale, *Green Chem.*, 2012, **14**, 2790-2798.
43. V. s. Á, Z. W. Qu, G. J. Kroes, J. Rossmeisl and J. K. Nørskov, *J, Phys. Chem. C*, 2008, **112**.
44. L. Liu, X. Zhao, H. Sun, C. Jia and W. Fan, *ACS Appl. Mater. Interfaces*, 2013, **5**, 6893-6901.
45. Z. The Journal of …Zongyan, L. Zhaosheng and Z. Zhigang, *J. Phys. Chem. C*, 2013, **117**, 6172−6184.
46. J. Wang, W. Luo, J. Feng, L. Zhang, Z. Li and Z. Zou, *Phys. Chem. Chem. Phys.*, 2013, **15**, 16054-16064.
47. H. Ye, G. Chen, H. Niu, Y. Zhu, L. Shao and Z. Qiao, *J. Phys. Chem. C*, 2013, **117**, 15976-15983.
48. Y. Wang, R. Kovacik, B. Meyer, K. Kotsis, D. Stodt, V. Staemmler, H. Qiu, F. Traeger, D. Langenberg, M. Muhler and C. Woll, *Angew. Chem. Int. Ed.*, 2007, **46**, 5624-5627.
49. X. Jianping and F. Thomas, *J. Phys. Chem. C*, 2013, **117**, 1804–1808.
50. J. B. Lopes Martins, E. Longo, O. D. Rodríguez Salmon, V. A. A. Espinoza and C. A. Taft, *Chem. Phys. Lett.*, 2004, **400**, 481-486.
51. Y.-F. Zhao, R. Rousseau, J. Li and D. Mei, *J. Phys. Chem. C*, 2012, **116**, 15952-15961.
52. N. V. Minh and V. N. Tuoc, *Proc. Natl. Conf. Theor. Phys.*, 2010, **35**, 101-108.
53. Z.-Y. Zhao, *J. Phys. Chem. C*, 2014, **118**, 4287-4295.
54. Y. Yang, M. N. Weaver and K. M. Merz, *J. Phys. Chem. A*, 2009, **113**, 9843-9851.
55. B. K. Carpenter, *J. Phys. Chem. A*, 2006, **111**, 3719-3726.
56. Y. X. Pan, C. J. Liu, D. Mei and Q. Ge, *Langmuir*, 2010, **26**, 5551-5558.
57. V. Kalamse, N. Wadnerkar, A. Deshmukh and A. Chaudhari, *Int. J Hydrogen Energy*, 2012, **37**, 3727-3732.
58. E. D. Glendening, A. E. Reed, J. E. Carpenter and F. Weinhold, NBO Version 3.1.
59. M. J. Frisch, G. W. Trucks, H. B. Schlegel, G. E. Scuseria, M. A. Robb, J. R. Cheeseman, G. Scalmani, V. Barone, B. Mennucci, G. A. Petersson, H. Nakatsuji, M. Caricato, X. Li, H. P. Hratchian, A. F. Izmaylov, J. Bloino, G. Zheng, J. L. Sonnenberg, M. Hada, M. Ehara, K. Toyota, R. Fukuda, J. Hasegawa, M. Ishida, T. Nakajima, Y. Honda, O. Kitao, H. Nakai, T. Vreven, J. A. Montgomery Jr., J.

E. Peralta, F. Ogliaro, M. J. Bearpark, J. Heyd, E. N. Brothers, K. N. Kudin, V. N. Staroverov, R. Kobayashi, J. Normand, K. Raghavachari, A. P. Rendell, J. C. Burant, S. S. Iyengar, J. Tomasi, M. Cossi, N. Rega, N. J. Millam, M. Klene, J. E. Knox, J. B. Cross, V. Bakken, C. Adamo, J. Jaramillo, R. Gomperts, R. E. Stratmann, O. Yazyev, A. J. Austin, R. Cammi, C. Pomelli, J. W. Ochterski, R. L. Martin, K. Morokuma, V. G. Zakrzewski, G. A. Voth, P. Salvador, J. J. Dannenberg, S. Dapprich, A. D. Daniels, Ö. Farkas, J. B. Foresman, J. V. Ortiz, J. Cioslowski and D. J. Fox, *Journal*, **2009**, Gaussian Revision C.01.

60. S. J. Clark, M. D. Segall, C. J. Pickard, P. J. Hasnip, M. I. J. Probert, K. Refson and M. C. Payne, *Z. Kristallogr.*, 2005, **220**, 567-570.
61. N. P. Herring, L. S. Panchakarla and M. S. El-Shall, *Langmuir*, 2014, **30**, 2230-2240.
62. Y. Jingyun, L. Changjun, M. Donghai and G. Qingfeng, *ACS Catalysis*, 2013, **3**.
63. S. Gangarapu, A. T. M. Marcelis and H. Zuilhof, *ChemPhysChem*, 2013, **14**, 3936-3943.
64. J. Ye, C. Liu and Q. Ge, *J. Phys. Chem. C*, 2012, **116**, 7817-7825.
65. X. Sun, X. Cao and P. Hu, *Sci. China Chem.*, 2015, DOI: 10.1007/s11426-015-5340-y, 1-12.
66. X. Nie, W. Luo, M. J. Janik and A. Asthagiri, *J. Catal.*, 2014, **312**, 108-122.
67. Y. Yang and D. Cheng, *J. Phys. Chem. C*, 2013, **118**, 250-258.
68. Y.-F. Li and A. Selloni, *ACS Catalysis*, 2014, **4**, 1148-1153.
69. X. Lü, X. Xu, N. Wang, Q. Zhang, M. Ehara and H. Nakatsuji, *J. Phys. Chem. B*, 1999, **103**, 2689-2695.
70. T. Inui and T. Takeguchi, *Catal. Today*, 1991, **10**, 95-106.
71. W. H. Doh, P. C. Roy and C. M. Kim, *Langmuir*, 2010, **26**, 16278-16281.
72. G. Peng, S. J. Sibener, G. C. Schatz, S. T. Ceyer and M. Mavrikakis, *J. Phys. Chem. C*, 2012, **116**, 3001-3006.
73. A. A. Peterson, F. Abild-Pedersen, F. Studt, J. Rossmeisl and J. K. Norskov, *Energy Environ. Sci.*, 2010, **3**, 1311-1315.

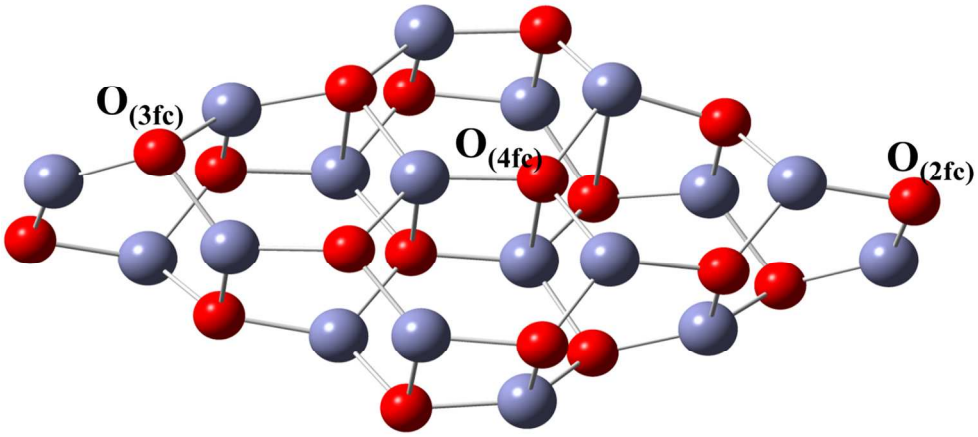

Figure 1. Schematic representation of optimized $Zn_{18}O_{18}$ cluster.

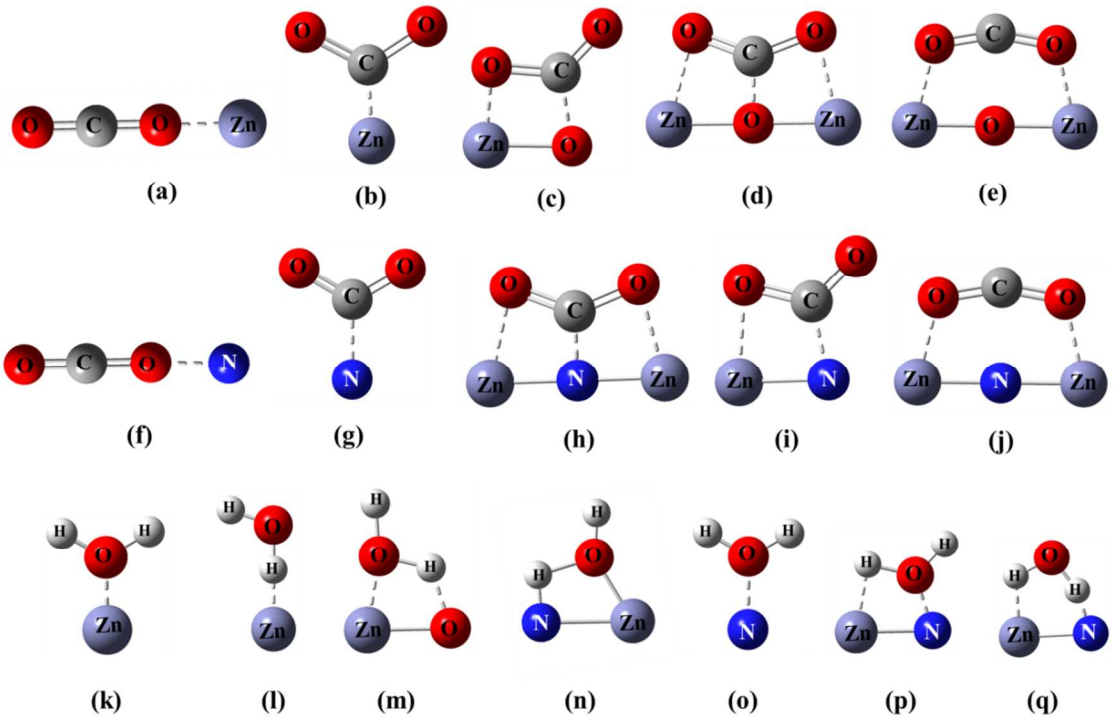

Figure 2. Schematic representation of the various adsorption modes for CO_2, [(a)-(j)] and for H_2O, [(k)-(q)] on stoichiometric $Zn_{18}O_{17}$:N cluster.

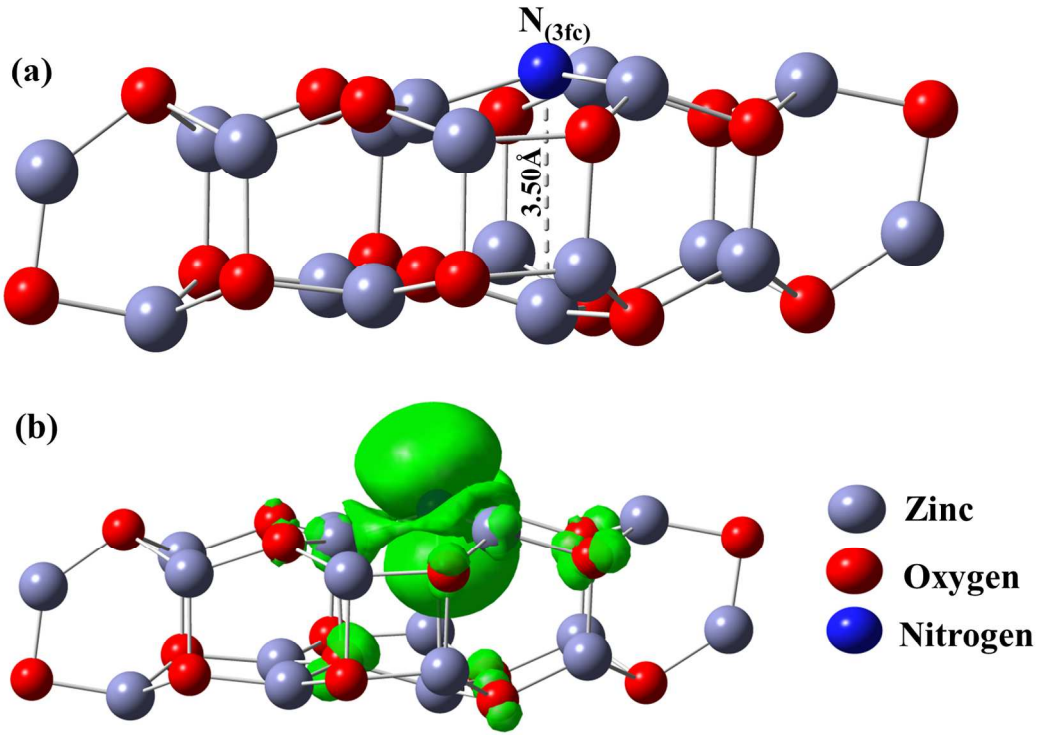

Figure 3. Optimized structure of (a) $Zn_{18}O_{17}$:N and (b) spin density distribution in $Zn_{18}O_{17}$:N.

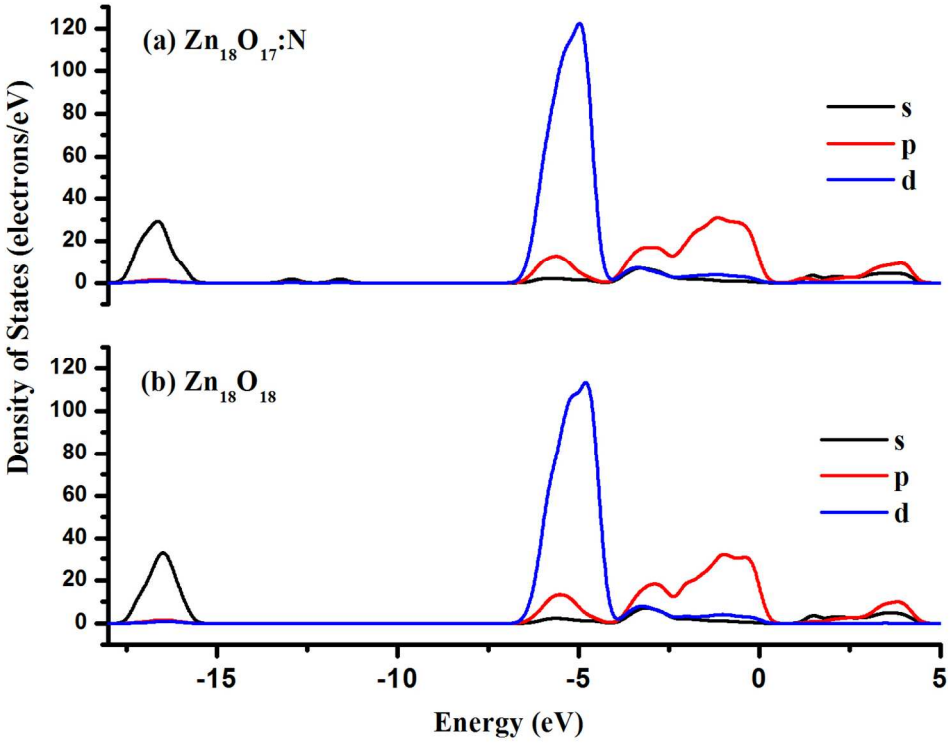

Figure 4. Partial Density of States population of (a) Nitrogen doped zinc oxide and (b) Pure ZnO clusters.

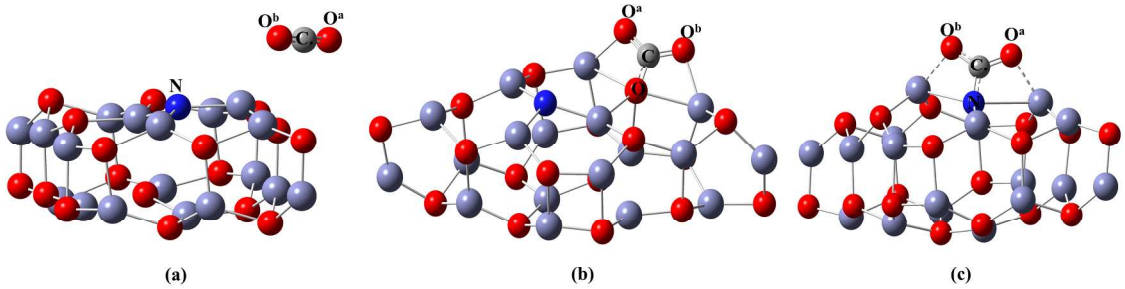

Figure 5. Optimized structures for the various coordinative adsorption modes of CO_2leading to (a) physisorption (b) bridge tridentate carbonate and (c) bridge tridentate carbamate on $Zn_{18}O_{17}$:N.

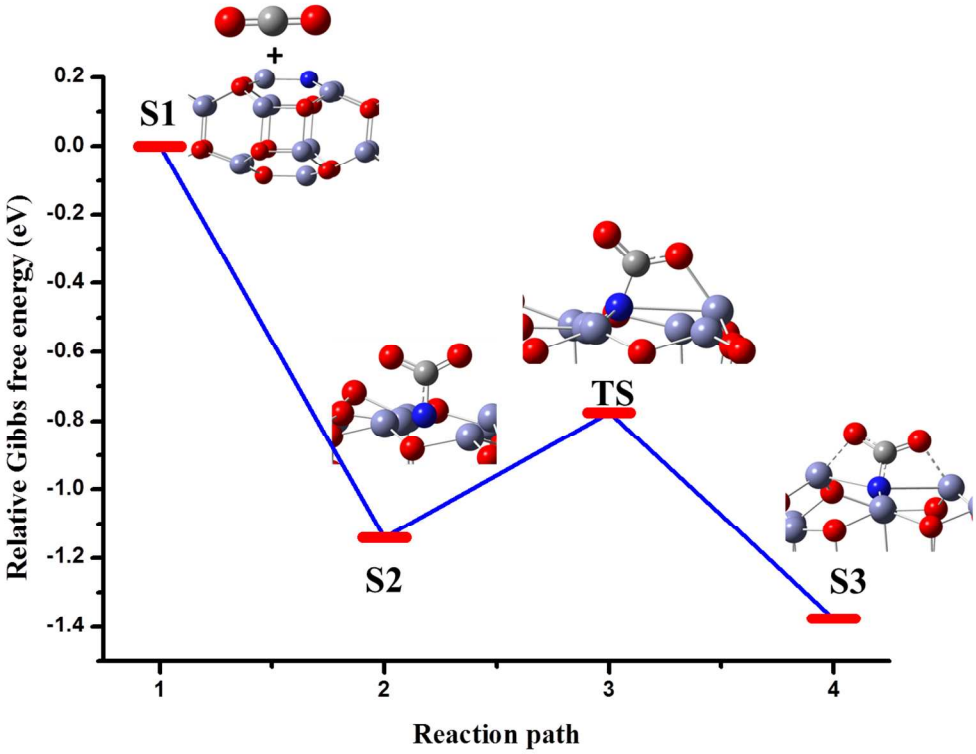

Figure 6. Relative Gibbs **e**nergy profile for the reaction of CO_2 to CO_2^- on the surface of stoichiometric $Zn_{18}O_{17}$:N with the corresponding structures to form N-carboxylate.

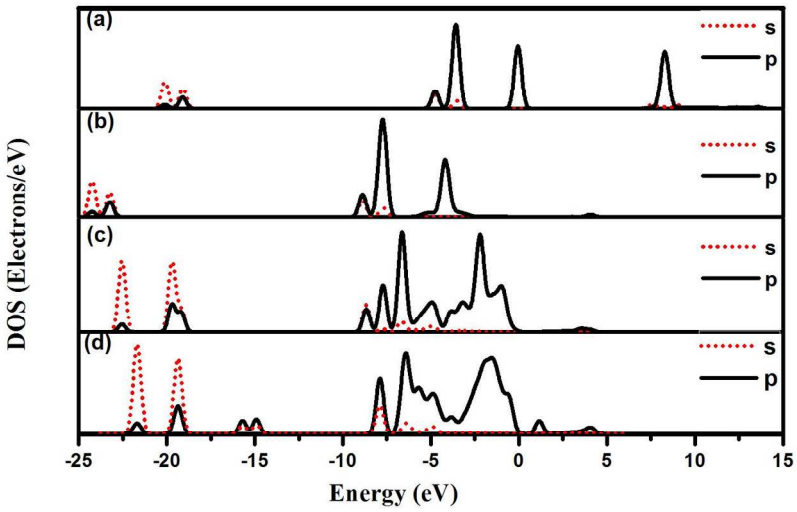

Figure 7. Partial density of states population of (a) free CO_2, (b) physisorption (c) tridentate carbonate and (d) tridentate carbamate species on nitrogen doped zinc oxide clusters.

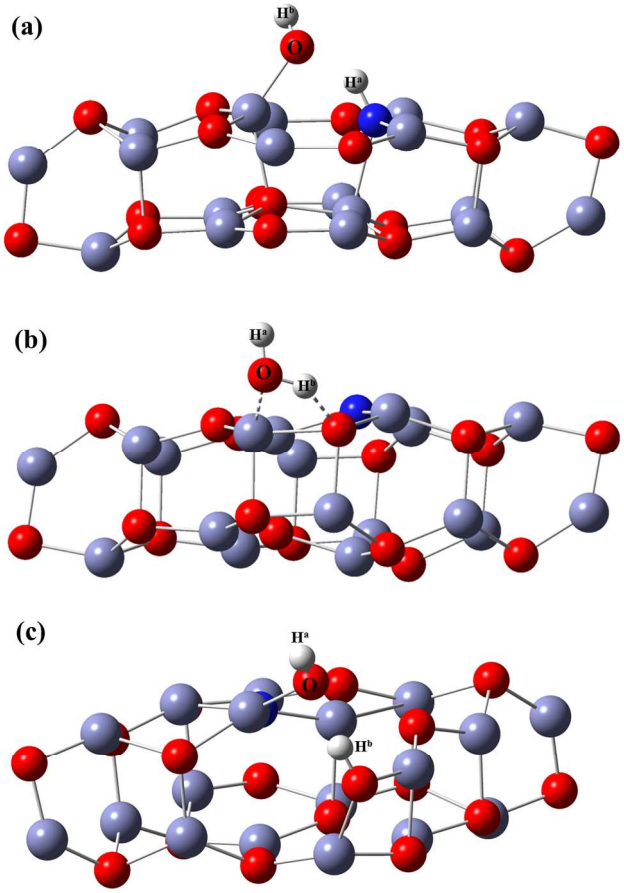

Figure 8. Optimized structures of H_2O adsorbed on $Zn_{18}O_{17}$:N, (a) & (c) dissociative and (b) molecular adsorption.

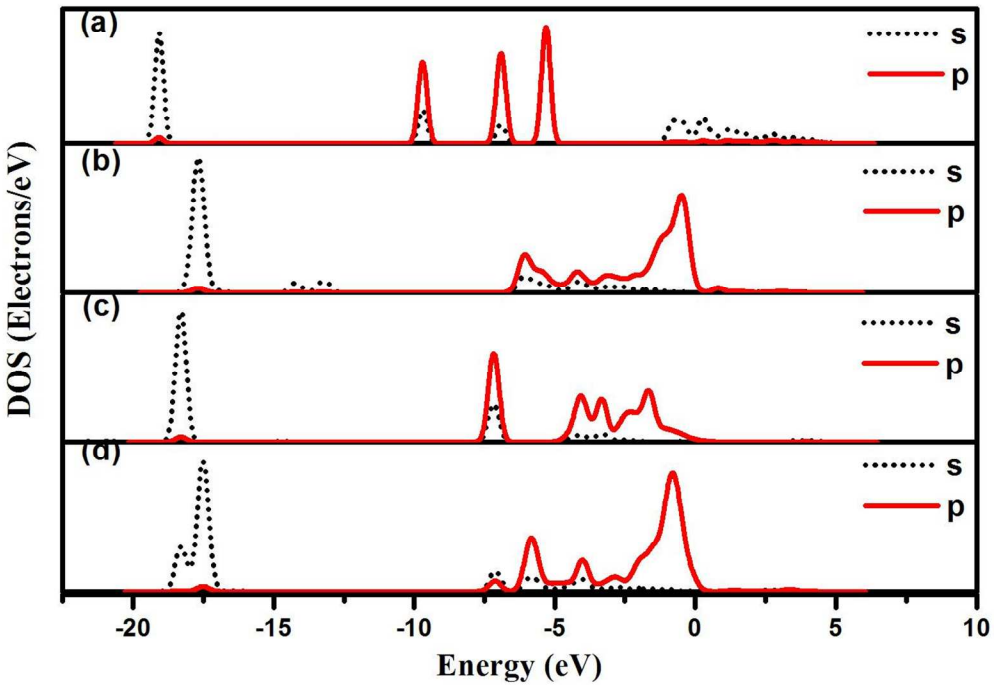

Figure 9. Partial density of states population of (a) free H_2O, (b) & (d) dissociative and (c) molecular adsorption.

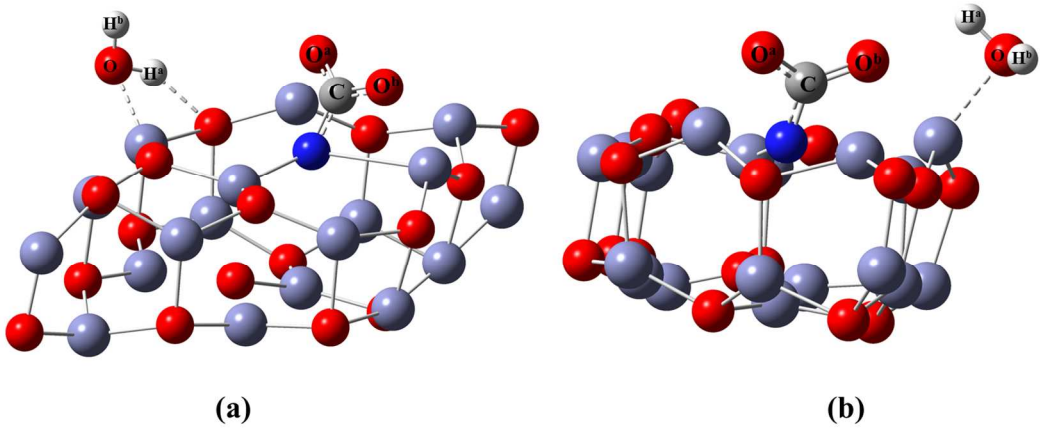

Figure 10. Optimized structures for the coadsorption of CO_2 and H_2O on $Zn_{18}O_{17}N$ (a) &(b).

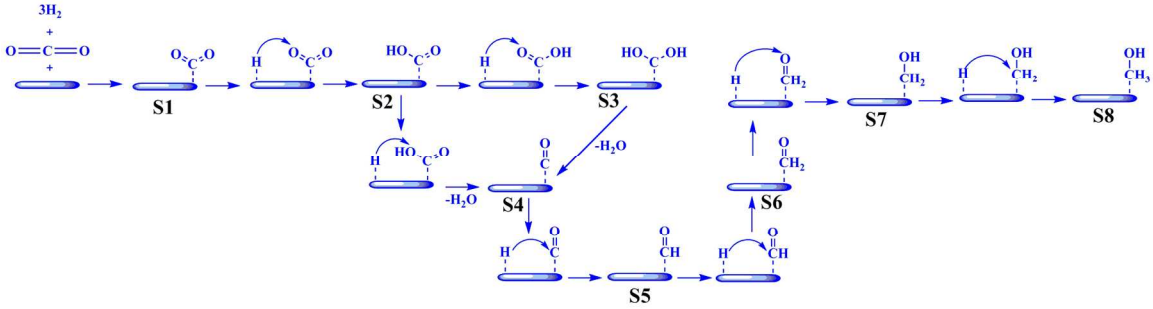

Figure 11. Reaction path for reaction of CO_2 with H_2 to form CH_3OH on $Zn_{18}O_{17}$:N surface.

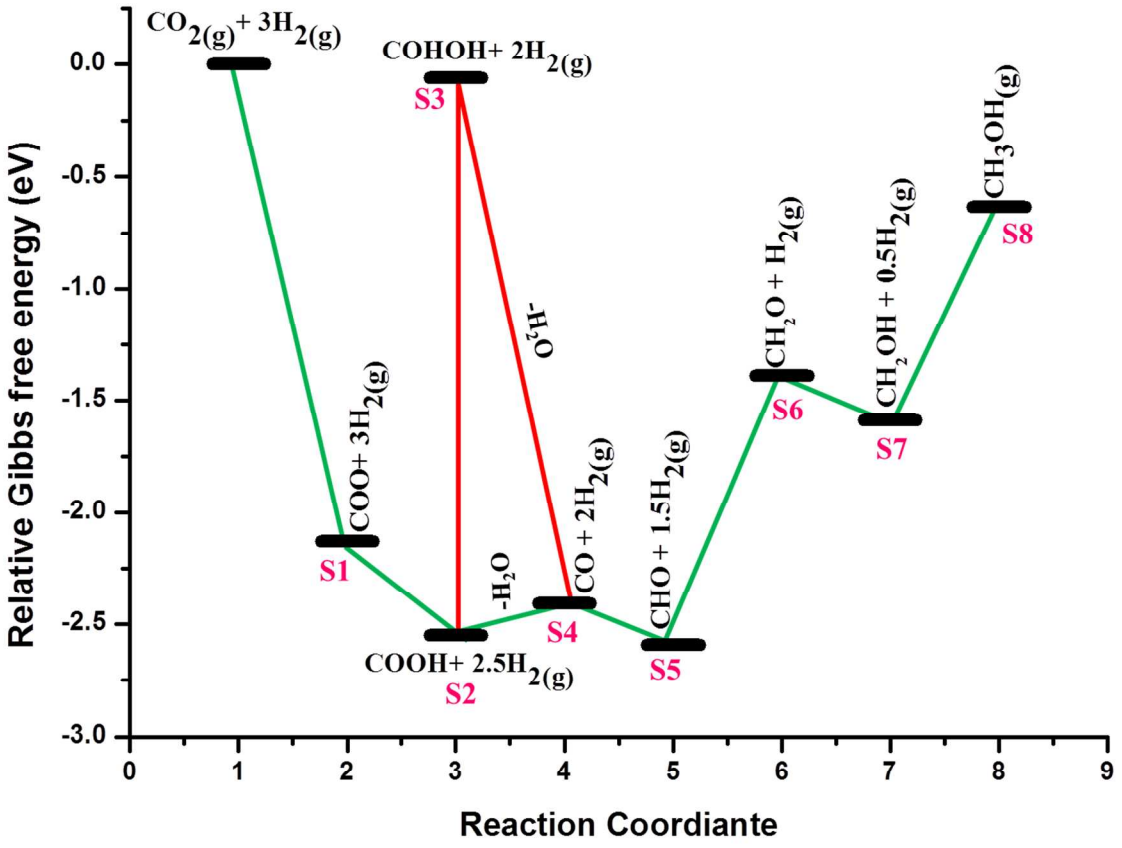

Figure 12. Relative Gibbs free energy profile for reaction of CO_2 with H_2 to form CH_3OH on $Zn_{18}O_{17}$:N surface.

Table 1. Computed CO2 adsorption energies in eV (ΔE), Bond length in Å (l), Bond angle in ° (Θ), Chemisorption distance in Å (d) and NBO charges in e (q) of CO_2 on $Zn_{18}O_{17}$:N

Configuration	ΔE	d	l(C-O^a)	l(C-O^b)	Θ	Q			
						N	C	O^a	O^b
CO_2	-	-	1.16	1.16	179.9	-	1.069	-0.535	-0.535
A	-0.48	2.5	1.16	1.17	176.8	-1.455	1.115	-0.576	-0.506
B	-1.14	1.33	1.27	1.27	122.9	-1.472	1.081	-0.833	-0.803
C	-1.86	1.35	1.28	1.29	123.7	-0.840	0.867	-0.797	-0.808

Table 2. Computed H_2O adsorption energies in eV (ΔE), Bond length in Å (l), Bond angle in ° (Θ), and NBO charge in e (q) for associative adsorption of H_2Oon $Zn_{18}O_{17}$:N

Configuration	ΔE	l(H-O^a)	l(H-O^b)	Θ	q			
					N	O	H^a	H^b
H_2O	-	0.96	0.96	104.7		-0.958	0.479	0.479
A	0.02	-	0.96	-	-1.237	-1.230	0.401	0.478
B	-0.77	0.96	0.99	107.7	-1.451	-0.999	0.498	0.535
C	-0.44	0.96	-	108.5	-1.495	-1.006	0.515	0.515

Table 3. Computed CO_2 and H_2O coadsorption energies in eV (ΔE), Bond length in Å (l), Bond angle in ° (Θ), Chemisorption distance in Å (d) and Mullikan charge in (q) for coadsorption of $CO_2$and H_2Oon $Zn_{18}O_{17}$:N

Model	ΔE	l(O-H^a)	l(O-H^b)	Θ	l(C-O^a)	l(C-O^b)	Θ	Q					
								O	H^a	H^b	C	O^a	O^b
a	-2.27	0.99	0.96	107.7	1.28	1.28	122.6	-1.001	0.536	0.513	0.868	-0.813	-0.807
b	-2.15	0.97	0.96	106.1	1.29	1.28	122.4	-0.971	0.525	0.511	0.875	-0.812	-0.835

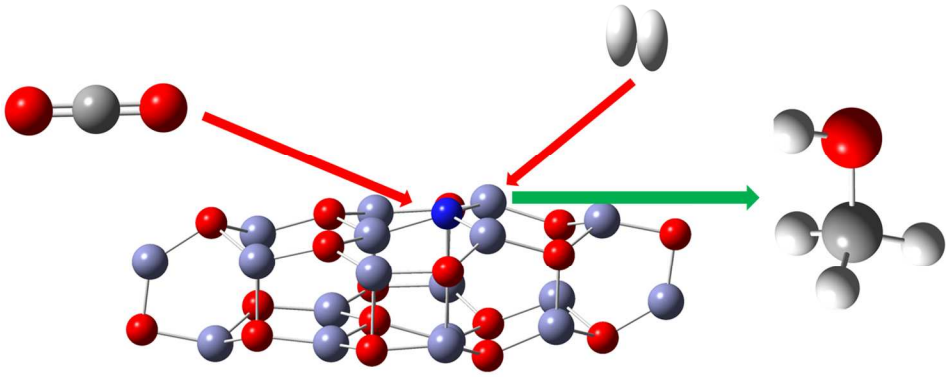

Table of Contents